OH- and CH-Stretching Overtone Spectra of Catechol

Henrik G. Kjaergaard,* Daryl L. Howard, Daniel P. Schofield, and Timothy W. Robinson

Department of Chemistry, University of Otago, P.O. Box 56, Dunedin, New Zealand

Shun-ichi Ishiuchi and Masaaki Fujii

Institute for Molecular Science, Myodaiji, Okazaki 444-8585, Japan

Received: June 29, 2001; In Final Form: October 22, 2001

We have recorded the CH-, OH-, and OD-stretching fundamental and overtone spectra of catechol (1,2-dihydroxybenzene, pyrocatechol) and selectively deuterated catechol. Conventional and intracavity photoacoustic spectroscopy were used to record room temperature spectra of catechol in solution and in the vapor phase, whereas nonresonant ionization detected spectroscopy was used to study catechol in a supersonic jet. The spectra can be explained in terms of a local mode model with one oscillator for each of the nonequivalent CH, OH, or OD bonds. Intensities of the CH-, OH-, and OD-stretching transitions were calculated with an anharmonic oscillator local mode model and ab initio determined dipole moment functions. Our simple calculations are in good agreement with the observed intensities. Line widths in the jet-cooled spectra are discussed in terms of intramolecular vibrational redistribution. The spectroscopic and theoretical results are in agreement with a relatively weak intramolecular hydrogen bond.

Introduction

The structure of the electronic ground state of catechol (1,2-dihydroxybenzene, pyrocatechol) has been determined by various methods such as microwave spectroscopy,[1,2] X-ray diffraction,[3,4] infrared and Raman spectroscopy,[5−10] and more recently, by ab initio and density functional theory calculations.[11−13] The consensus of these studies is that the electronic ground state of catechol has a planar geometry of C_s symmetry as depicted in Figure 1. The two hydroxyl groups in catechol form an intramolecular hydrogen bond, with one hydroxyl group acting as the hydrogen donor or bonding group, OH_b, and the other acting as the acceptor or free group, OH_f. The experimental hydrogen bond energy of catechol is 2.3 kcal/mol[14] whereas ab initio and density functional theory (DFT) calculations yield a bond energy of approximately 4 kcal/mol at various levels of theory.[11,12] The theoretical hydrogen bond strength is determined as the energy difference between the conformer in Figure 1, and the conformer in which the OH_b hydroxyl group is rotated by 180° to minimize steric interaction. This intramolecular hydrogen bond is relatively weak compared to intermolecular hydrogen bonds.[15] For example, in the water dimer the hydrogen bond energy is about 5 kcal/mol.[15]

We have recorded the CH-, OH-, and OD-stretching fundamental and overtone spectra of catechol-d_0, -d_1, and -d_2 in a supersonic jet, in the vapor phase, and in a CS_2 solution. The vapor pressure of catechol is low (approximately 0.03 Torr at 20 °C) and overtone transitions in catechol have not previously been recorded. Due to the low vapor pressure, sensitive spectroscopic techniques have to be used to record the vapor phase overtone spectra of catechol. Room temperature vapor phase overtone spectra have previously been recorded for the solids phenol[16] and naphthalene[17] with intracavity laser photoacoustic spectroscopy (ICL-PAS), and spectra of jet-cooled phenol have recently been recorded by nonresonant ionization detected (NID) spectroscopy.[18,19] We have used the sensitive ICL-PAS and NID techniques to record the overtone spectra of catechol. We compare our present results for catechol with previous results obtained for phenol.[16,18,19]

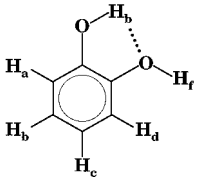

Figure 1. B3LYP/6-311++G(2d,2p) optimized structure of catechol is planar with the following bond lengths in Å: $OH_b = 0.9644$, $OH_f = 0.9608$, $CH_a = 1.0808$, $CH_b = 1.0807$, $CH_c = 1.0805$, $CH_d = 1.0835$.

Overtone spectra are successfully explained within the local mode model of molecular vibration.[20−22] The peak positions in XH-stretching (where X = C, N, O, etc.) overtone spectra can be calculated with a harmonically coupled anharmonic oscillator (HCAO) local mode model with reasonable accuracy.[22,23] The local mode parameters can be determined from selected observed transitions. Combined with ab initio calculated dipole moment functions (DMFs) the HCAO local mode model has been successful in the calculation of XH-stretching overtone intensities.[17,24,25] Recently we have used ab initio determined local mode parameters and DMFs with the HCAO local mode model to simulate overtone spectra of species for which the spectra have not yet been observed.[26−28]

In this paper, we have calculated the CH-, OH-, and OD-stretching fundamental and overtone intensities for catechol. Because all the CH, OH (OD) bonds in catechol are nonequivalent and the coupling between them is expected to be very small,[25] the HCAO local mode model reduces to that of a simple isolated anharmonic oscillator (AO) local mode model for each of the nonequivalent bonds. We have compared our theoretical and experimental intensity results.

* To whom correspondence should be addressed. E-mail: henrik@alkali.otago.ac.nz. Fax: +64-3-479-7906.

10.1021/jp0124847 CCC: $22.00
Published on Web 12/14/2001

We have previously found that the overtone transitions of the hydrogen bonded OH bond in hydrated complexes are sensitive to the choice of ab initio method.[26,28] However, no overtone spectra of hydrated complexes are available for comparison yet. We have considered the internal hydrogen bond in catechol for which we could both measure and calculate the overtone transitions in an attempt to improve our understanding of the hydrogen bond.

Experimental Section

Crystalline catechol (Aldrich, 99+% or Wako, 99%) was used without any further purification. The room-temperature vapor phase spectrum of catechol was recorded in the $\Delta v_{OH} = 3$ region with ICL-PAS at the University of Otago. Our version of ICL-PAS is similar to other versions that have been described previously.[29,30] Briefly, a Coherent Innova Sabre argon ion laser running at all lines with 16 W of output power was used to pump a Coherent 890 broadband titanium:sapphire laser with long-wave optics. The photoacoustic cell contained a Knowles Electronics, Inc. EK3132 electret microphone, and its signal was sent to a Stanford Research Systems SR830 lock-in amplifier. The laser was intensity modulated with a Stanford Research Systems SR540 mechanical chopper, and the lock-in amplifier was referenced to the modulation frequency. The laser output power was measured with a Coherent LaserMate-Q power meter fitted with a 1000:1 attenuator. The power meter output was sent to an Agilent 34401A digital multimeter after voltage integration with a resistor−capacitor (RC) circuit and was used to normalize the photoacoustic signal. The titanium: sapphire laser was tuned with a three plate birefringent filter rotated by a stepper motor attached to a micrometer screw. The three plate birefringent filter gives a line width of 1 cm^{-1}. Our photoacoustic apparatus is computer controlled through a National Instruments IEEE interface. The wavelength calibration of the scans was conducted with a Burleigh WA-1000 wavemeter. The photoacoustic cell was filled with argon buffer gas at a pressure of 180 Torr to increase the photoacoustic signal.[31,32] The absolute absorbance of a sample is not known with our ICL-PAS apparatus; however, relative intensities can be obtained from the ICL-PAS spectra.

The spectrum of jet-cooled catechol was recorded with NID spectroscopy at the Institute for Molecular Science. The experimental details of NID spectroscopy have been described in detail elsewhere.[18,19] Briefly, NID is a IR−NIR/UV double resonance spectroscopic technique which selectively detects a vibrationally excited molecule. The UV laser radiation is fixed to a wavelength such that only vibrationally excited molecules generated by the IR−NIR laser can be ionized by nonresonant 2-photon ionization. In the present study, the second harmonic of a Nd^{3+}:YAG laser (Spectra Physics: GCR-170) was used to pump a dye laser (Lumonics: HD-500) which was frequency doubled to produce 307.5 nm UV radiation. Tunable IR−NIR radiation was obtained by the differential mixing technique or from an OPO laser. The second harmonic of the YAG laser (Continuum:Powerlite 8010) and the output of the dye laser (620−670 nm) were differentially mixed in a $LiNdO_3$ crystal (Inrad: AUTO-TRACKER−II) to give radiation in the 3 μm region. Differential mixing between the fundamental of the YAG laser and the dye laser produced NIR radiation in the 2.6−1.8 μm region. The OPO laser (Spectra Physics:MOPO−HF/GCR−PRO250) was used to cover the 1.8−0.7 μm region. The line width of the IR/NIR laser was less than 0.1 cm^{-1} in all regions. Both UV and IR−NIR beams were coaxially introduced into a vacuum chamber where they crossed a supersonic jet. The UV laser was delayed by 50 ns with respect to the IR−NIR laser. The generated cations were pushed into a detector chamber by a repeller at an appropriate voltage (typically 15 V/cm) and were detected by a channel multiplier (Murata Ceratron) through a quadrupole mass filter (EXTREL). The signal was amplified by a preamplifier (EG&G PARC 115) and was integrated by a digital boxcar (EG&G PARC 4420/4422). The integrated signal was recorded as a function of the IR−NIR laser wavelength. Vapor of catechol heated to 70 °C was seeded in He gas (2 atm) and the mixture was expanded into the vacuum chamber through a solenoid valve. Catechol-d_1 and -d_2 were obtained from mixing catechol-d_0 with D_2O. The spectra of catechol-d_0, -d_1 and -d_2 were separated by the quadrupole mass filter.

Catechol was dissolved in CS_2 to produce a 0.004 59 M solution used to record the fundamental CH- and OH-stretching region and a 0.007 23 M solution used to record the overtone regions. Partially deuterated catechol (~60% atom D) was synthesized by adding excess D_2O to catechol and stirring for 2 days, and the solvent was evaporated. The solution spectra of an approximately 0.0073 M solution of partially deuterated catechol in CS_2 were recorded with a 1-cm quartz cell for the fundamental region and a 10-cm quartz cell for the overtone regions. Equivalent quartz cells filled with CS_2 were used in the reference beam path for the overtone scans. A Varian Cary 500 UV−visible-NIR spectrophotometer was used to record the solution phase spectra. The spectra were recorded with a fixed spectral bandwidth (slit width) of 1.0 nm and at the ambient temperature of 22 °C. The fundamental regions were also recorded with a Bruker Equinox 55 FTIR fitted with a KBr beam splitter and a DTGS detector. The FTIR spectra were recorded with a resolution of 1 cm^{-1} and 128 scans.

Galactic Grams/32 (v5.03) software was utilized for spectral curve-fitting of ICL-PAS and solution phase spectra. Spectral bands were curve-fitted with Gaussian−Lorentzian mixture functions to a linear baseline, and no other constraints were applied to the curve-fitting procedure. The NID spectra were deconvoluted into Lorentzian peaks with a linear baseline with the Igor Pro (v. 3.16) curve-fitting program.

Theory and Calculations

The dimensionless oscillator strength f of a transition from the ground vibrational state g to an excited vibrational state e is given by[24,33]

$$f = 4.702 \times 10^{-7}\ [\mathrm{cm}^{-1}\ \mathrm{D}^{-2}]\tilde{\nu}_{eg}|\vec{\mu}_{eg}|^2 \qquad (1)$$

where $\tilde{\nu}_{eg}$ is the transition frequency in cm^{-1} and $\vec{\mu}_{eg} = \langle e|\vec{\mu}|g\rangle$ is the transition dipole moment in Debye (D).

The catechol structure in Figure 1 has two nonequivalent OH bonds and four nonequivalent CH bonds. The coupling between CH- or OH-stretching oscillators is usually only significant if the oscillators share a common heavy atom.[25,34] Thus, the CH-stretching overtone vibrations in catechol can to a good approximation be described by four isolated nonequivalent local modes and similarly the OH-stretching vibrations as two isolated nonequivalent local modes. The wave functions of the CH- and OH-stretching modes are each described by a Morse oscillator with the Hamiltonian

$$(H - E_{|0\rangle})/hc = v\omega - (v^2 + v)\tilde{\omega}x \qquad (2)$$

where $E_{|0\rangle}$ is the energy of the vibrational ground state and $\tilde{\omega}$ and $\tilde{\omega}x$ are the local mode frequency and anharmonicity of the

TABLE 1: Scaling Factors for Local Mode Parameters[a]

	HF/6-311++G(2d,2p)		B3LYP/6-311++G(2d,2p)	
bond	sf $\tilde{\omega}$	sf $\tilde{\omega}x$	sf $\tilde{\omega}$	sf $\tilde{\omega}x$
OH	0.912	0.912	0.996	0.872
CH	0.946	0.909	0.990	0.861

[a] Scaling factors were obtained as the ratio of experimental local mode parameters to calculated parameters for the OH bond in phenol and for the CH bond in benzene.

oscillator, respectively. The associated Morse oscillator eigenfunctions are required to calculate the transition dipole moment.

The DMF for each of the local modes is approximated as a series expansion in the internal CH− or OH-stretching displacement coordinate, q, and can be written as

$$\vec{\mu}(q) = \sum_{i=1}^{5} \vec{\mu}_i q^i \tag{3}$$

The expansion coefficients

$$\vec{\mu}_i = \frac{1}{i!}\frac{\partial^i \vec{\mu}}{\partial q^i}\bigg|_e \tag{4}$$

are determined from ab initio or density functional theory (DFT) calculations of the dipole moment at the equilibrium geometry and at geometries in which the bond is displaced from its equilibrium. The dipole moment is calculated at nine points obtained by stretching the bond by ±0.2 Å in steps of 0.05 Å. All ab initio and DFT calculations were performed with Gaussian 94.[35] The optimized geometry was confirmed by a frequency calculation that yielded no imaginary eigenvalues. The calculated harmonic frequencies are given as Supporting Information in Table 1S. We have used the self-consistent-field Hartree−Fock (HF) and the B3LYP level of theory both with the 6-311++G(2d,2p) basis set.

The OD-stretching vibrations in the deuterated catechol are treated similarly to the OH-stretching vibrations. Within the Born−Oppenheimer approximation, the calculated DMF is identical for OH and OD bonds. The change in reduced mass leads to changes in the local mode parameters and thus in the transition dipole moment.

Scaling Factors. The local mode parameters, $\tilde{\omega}$ and $\tilde{\omega}x$, are typically obtained from a fit of the experimentally observed local mode peak positions $\tilde{\nu}$ to a two-parameter Morse oscillator energy expression

$$\tilde{\nu}/\upsilon = \tilde{\omega} - (\upsilon + 1)\tilde{\omega}x \tag{5}$$

We have used this method to determine the local mode parameters for the OH- and OD-stretching modes. For the four CH-stretching modes, it has not been possible to resolve four isolated transitions. Thus, it has not been possible to determine the experimental CH-stretching local mode parameters. However, the local mode parameters can be obtained from ab initio calculated anharmonic potential energy curves along the CH-stretching coordinates.[26,36] To calculate the local mode parameters, both the second and the third-order derivatives of the potential energy curve are required.[26,36] Ab initio and DFT calculations typically overestimate fundamental vibrational frequencies, so an empirical scaling factor is usually applied to obtain better agreement with experimental observations.[37] We have used a similar technique to scale the calculated local mode parameters. Appropriate scaling factors for the CH bonds were acquired by comparison of calculated $\tilde{\omega}$ and $\tilde{\omega}x$ values for benzene, a molecule for which the experimental vapor phase local mode parameters have been determined.[38] We have also determined scaling factors for the OH bonds in catechol from experimental and calculated local mode parameters of the OH bond in phenol. The determined scaling factors are given in Table 1. We have compared our experimentally obtained local mode parameters of the OH bonds in catechol with the scaled ab initio calculated values in Table 2.

TABLE 2: Observed OH-Stretching Peak Positions and Experimental Local Mode Parameters (in cm^{-1})[a]

method	bond	$\Delta\upsilon = 1$	$\Delta\upsilon = 2$	$\Delta\upsilon = 3$	$\Delta\upsilon = 4$	$\tilde{\omega}$	$\tilde{\omega}x$
NID	OH_b	3611	7063	10318	13406	3788 ± 7	87.1 ± 1.8
	OH_f	3668	7188	10512	13679	3839 ± 8	83.5 ± 2.2
PAS	OH_b			10317			
	OH_f			10511			
CS_2	OH_b	3562	6949	10159		3737 ± 0.6	87.7 ± 0.2
	OH_f	3594	7037	10293		3759 ± 11	81.5 ± 3.5
calc.[b]	OH_b	3617	7066	10346	13457	3786	84.4
	OH_f	3670	7172	10507	13673	3838	83.9

[a] Uncertainties given are one standard deviation. [b] Calculated with the B3LYP/6-311++G(2d,2p) method and the scaling factors from Table 1.

Results and Discussion

The optimized geometry of catechol is shown in Figure 1 which also shows the labeling used. The B3LYP/6-311++G(2d,2p) calculated CH and OH bond lengths are reported in the caption to Figure 1. The HF/6-311++G(2d,2p), B3LYP/6-31G(d), and B3LYP/6-311++G(2d,2p) geometry optimized parameters are given as Supporting Information in Table 2S. The HF/6-311++G(2d,2p) calculated bond lengths are all shorter than those calculated with the B3LYP method; however, the relative bond lengths are similar between the two methods. Individual vibrational overtone transitions of nonequivalent bonds are consistently resolved when the bond lengths differ by as little as 1 mÅ.[17,21] The three CH bonds labeled CH_a, CH_b, and CH_c have similar bond lengths, and the three individual CH-stretching transitions are unlikely to be well resolved experimentally. The CH_d bond is about 3 mÅ longer and the associated transition is expected to be resolved and occur at a lower wavenumber. Usually, the shorter the bond the higher the vibrational frequency.[21] The calculated bond length difference between the hydrogen-bonded OH bond, OH_b, and the free OH bond, OH_f, is 2.4 and 3.6 mÅ with the HF and B3LYP methods of calculation, respectively, in good agreement with other recent theoretical calculations.[11,12] Thus, with an OH bond length difference of more than 2 mÅ, we expect a significant splitting between the observed OH_b and OH_f vibrational transitions. The OH_f bond is shorter than the OH_b bond and we expect the OH_f-stretching transitions to lie at a higher wavenumber. Compared to our calculated OH bond length in phenol (0.9615 Å with B3LYP/6-311++G(2d,2p)), the OH_b bond is significantly longer and the OH_f bond is slightly shorter. An NID overview spectrum of jet-cooled catechol in the region 2800−14 200 cm^{-1} is shown in Figure 2. This spectrum clearly shows the two OH-stretching transitions. The transitions are well separated and the splitting increases with increasing $\Delta\upsilon_{OH}$. The CH-stretching transitions are not well resolved as predicted. The overview spectrum also clearly shows the increased dominance of the CH- and OH-stretching pure local modes as the transition wavenumber increases.

Jet-Cooled and Vapor Phase Spectra. The OH-stretching overtone spectra of jet-cooled catechol-d_0 in the regions corresponding to $\Delta\upsilon_{OH} = 2-4$ are shown in Figures 3−5. The

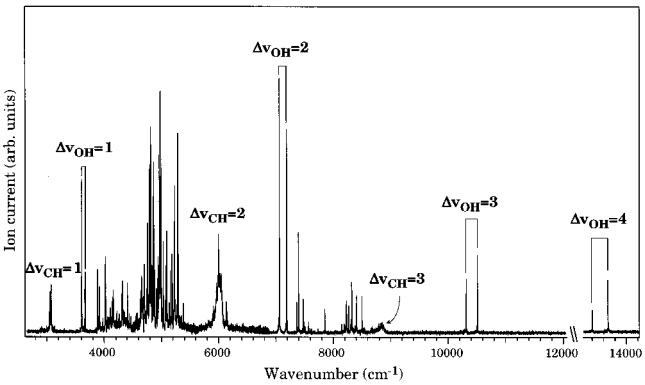

Figure 2. NID overview spectrum of jet-cooled catechol-d_0.

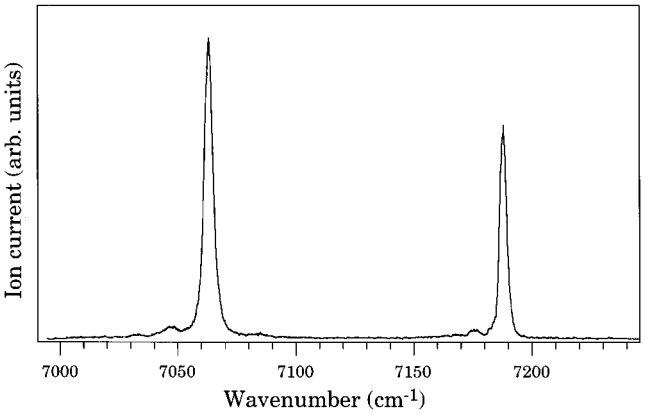

Figure 3. NID spectrum of jet-cooled catechol-d_0 in the $\Delta v_{OH} = 2$ region.

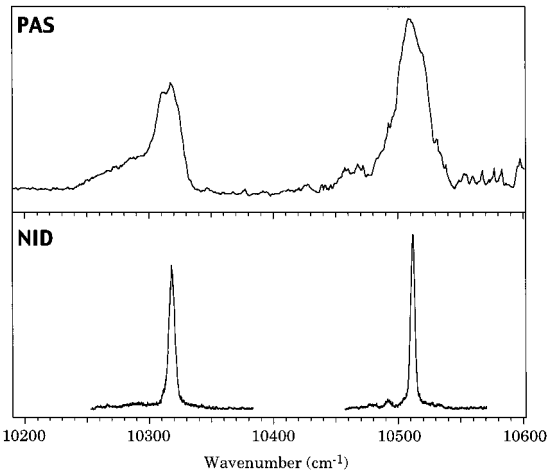

Figure 4. NID spectrum of jet-cooled and room-temperature vapor phase ICL-PAS spectrum of catechol-d_0 in the $\Delta v_{OH} = 3$ region.

room-temperature vapor phase ICL-PAS spectrum of catechol-d_0 in the $\Delta v_{OH} = 3$ region is also shown in Figure 4. The observed OH-stretching band positions are given in Table 2. The observed frequencies $\tilde{\nu}$ were fitted to eq 5 to determine the experimental local mode frequency $\tilde{\omega}$ and anharmonicity $\tilde{\omega}x$ the two nonequivalent OH oscillators in catechol. The experimentally determined local mode parameters are also given in Table 2 and compared to the calculated values. It is clear from the spectra that the two nonequivalent OH bonds are well resolved at each vibrational level. The low uncertainty of the local mode parameters indicates a good fit to eq 5 and support the assignment. Compared to the experimentally determined $\tilde{\omega}$ and $\tilde{\omega}x$ values for the OH-stretching oscillator in phenol[19] the

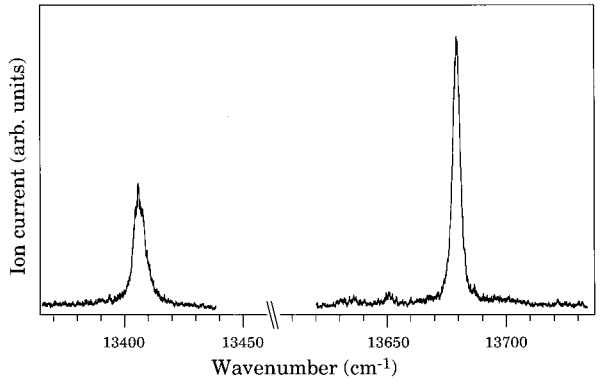

Figure 5. NID spectrum of jet-cooled catechol-d_0 in the $\Delta v_{OH} = 4$ region.

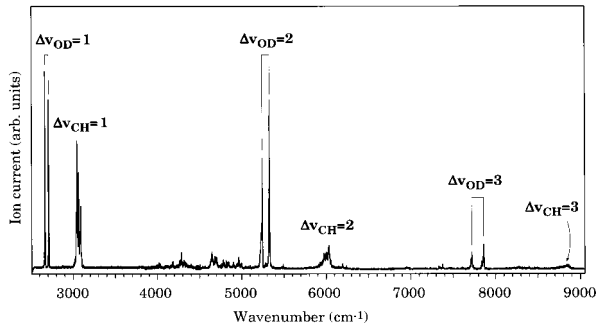

Figure 6. NID overview spectrum of jet-cooled catechol-d_2.

TABLE 3: Observed OD-Stretching Peak Positions and Experimental Local Mode Parameters (in cm^{-1})[a]

method	bond	$\Delta v = 1$	$\Delta v = 2$	$\Delta v = 3$	$\tilde{\omega}$	$\tilde{\omega}x$
NID	OD_b	2666	5245	7722	2759 ± 5	46.0 ± 1.4
	OD_f	2709	5329	7862	2797 ± 1	44.2 ± 0.2
CS_2	OD_b	2630	5167	7647	2709 ± 11	40.5 ± 3.5
	OD_f	2655	5216	7722	2734 ± 12	40.5 ± 3.8

[a] Uncertainties given are one standard deviation.

OH_b bond in catechol has a lower frequency and a higher anharmonicity as expected with hydrogen bonding. The OH_f bond is shifted to slightly higher frequency compared to the OH bond in phenol as expected from the bond lengths. Comparison of the jet-cooled and the room-temperature vapor phase spectra in Figure 4 show the expected significant increase in line width with the increase in temperature. However, the transition frequencies determined with the two different spectroscopic methods and at different temperatures agree well. The transition frequencies determined from curve-fitting of the two spectra differ by 1 cm^{-1} for both transitions. This difference is similar to the line width of the titanium:sapphire laser used in ICL-PAS.

The OD-stretching spectrum of catechol-d_2 in the $\Delta v_{OD} = 1$, 2 and 3 regions is shown in Figure 6 and the observed frequencies of the OD-stretching transitions are given in Table 3. Detailed spectra of the individual OD-stretching overtones are given as Supporting Information in Figures 1S−3S. The OD-stretching transitions show more structure than the corresponding OH-stretching transitions and could not be fitted with single Lorentzians. The frequency of each transition was taken as the center of the largest Lorentzian. The OD transition frequencies were fitted to eq 5, and the experimentally determined local mode parameters are given in Table 3. Comparison of the overview spectra of catechol-d_0 (Figure 2) and catechol-d_2 (Figure 6) reveals that there are fewer transitions to states other than the CH-, OH-, or OD-stretching local modes

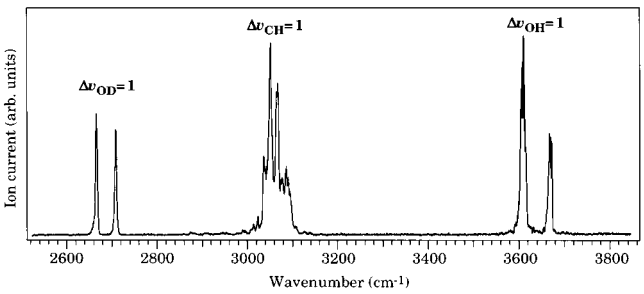

Figure 7. NID spectrum of jet-cooled catechol-d_1 in the OD-, CH-, and OH-stretching fundamental regions.

TABLE 4: Harmonic Frequencies (in cm^{-1}) and Oscillator Strengths in Catechol[a]

	B3LYP/6-31G(d)		B3LYP/6-311++G(2d,2p)	
mode	$\tilde{\nu}^b$	f	$\tilde{\nu}^c$	f
CH	3044	2.95×10^{-6}	3156	2.09×10^{-6}
CH	3070	1.18×10^{-6}	3181	7.42×10^{-7}
CH	3084	3.73×10^{-6}	3194	2.03×10^{-6}
CH	3093	1.84×10^{-6}	3203	1.25×10^{-6}
OH_b	3572	1.45×10^{-5}	3798	1.85×10^{-5}
OH_f	3626	1.06×10^{-5}	3850	1.50×10^{-5}

[a] Intensities from Gaussian94 assume a linear dipole in the normal coordinates. The intensities are converted to oscillator strengths by multiplication of the factor 1.876×10^{-7} mol km^{-1}. [b] The calculated frequencies are scaled by a common factor of 0.9613.[37] [c] Unscaled frequencies.

in the catechol-d_2 spectrum. This might be due to the higher coupling in catechol-d_2 thus spreading the intensity to a larger number of weak transitions which do not appear in the spectrum.

The OD-, CH-, and OH-stretching fundamental NID spectrum of jet-cooled catechol-d_1 is shown in Figure 7. Coupling between the two nonequivalent hydroxyl bonds would lead to frequency shifts between the transitions of the isolated OH bonds in the selectively deuterated molecule and the transitions of the coupled bonds in the nondeuterated molecule.[25] Little change in the OH-stretching frequencies is observed between the catechol-d_1 and -d_0 spectra. This absence of frequency shifts provides experimental evidence that the coupling between the two OH-stretching vibrations is very small. We have used Gaussian 94 to calculate the frequencies and intensities of the vibrational normal modes in catechol. Within Gaussian 94 the intensities are calculated with the use of a harmonic oscillator linear dipole approximation for each of the normal coordinates. These calculated frequencies and oscillator strengths of the CH- and OH-stretching normal modes in catechol are shown in Table 4. The harmonic frequency calculations show that the two OH-stretching normal modes are essentially isolated from each other as well as from the rest of the vibrational modes in the molecule, thus supporting the experimental evidence of little coupling between the two OH-stretching bonds. The frequencies calculated with the B3LYP/6-31G(d) method and scaled with a known common scaling factor[37] agree reasonably well with the observed CH- and OH-stretching transitions seen in Figure 7. The B3LYP/6-311++G(2d,2p) calculations are unscaled and show relatively similar frequencies compared to the B3LYP/6-31G(d) calculations, and small variations in intensities between the two methods are noted.

We have calculated the local mode parameters for each of the nonequivalent CH and OH bonds in catechol from the ab initio calculated anharmonic potential energy curves with both the HF/6-311++G(2d,2p) and the B3LYP/6-311++G(2d,2p) methods. The calculated local mode parameters were scaled with the scaling factors from Table 1 and are given in Table 5.

TABLE 5: Calculated Local Mode Parameters in Catechol (in cm^{-1})[a]

	HF/6-311++G(2d,2p)		B3LYP/6-311++G(2d,2p)	
bond	$\tilde{\omega}$	$\tilde{\omega}x$	$\tilde{\omega}$	$\tilde{\omega}x$
OH_b	3800	84.2	3786	84.4
OH_f	3830	84.2	3838	83.9
CH_a	3173	56.4	3165	57.0
CH_b	3166	57.0	3160	57.5
CH_c	3167	57.1	3162	57.6
CH_d	3139	57.2	3100	56.8

[a] Scaled with scaling factors from Table 1.

TABLE 6: Calculated CH-Stretching Peak Positions (in cm^{-1}) in Catechol[a]

bond	$\Delta v = 1$	$\Delta v = 2$	$\Delta v = 3$	$\Delta v = 4$
CH_a	3052	5989	8813	11 522
CH_b	3045	5975	8790	11 490
CH_c	3047	5979	8795	11 497
CH_d	2986	5859	8618	11 264

[a] Calculated with the B3LYP/6-311++G(2d,2p) local mode parameters from Table 5.

Comparison of the HF and B3LYP calculated local mode parameters shows reasonable agreement between the two methods employed. The main difference is the lower B3LYP frequencies of the CH_d and OH_b bonds. Comparison with the experimental values for the OH bonds in Table 2 shows very good agreement for the B3LYP calculated frequencies. The HF calculated frequencies are about 10 cm^{-1} higher and lower for the OH_b and OH_f bonds, respectively. Neither the HF nor the B3LYP method predicts the experimentally observed increase in anharmonicity of the OH_b bond. The agreement between calculated and observed OH-stretching transition frequencies as shown in Table 2 is reasonable. The larger disagreement between calculated and observed OH_b peak positions, with both the HF and the B3LYP methods, is an indication of the difficulties associated with electronic structure calculations of hydrogen bonds. The inadequacy of the B3LYP calculation and of DFT calculations in general when applied to strongly hydrogen-bonded systems has been noted previously.[15] However, for weak hydrogen bonds we have found that B3LYP calculations give results similar to calculations with the quadratic configuration interaction including single and double excitations (QCISD) method.[28] We have used both the HF and the B3LYP methods in our calculations on catechol with the knowledge that the B3LYP method possibly overestimates the red-shift and the HF method underestimates the red-shift of the hydrogen-bonded (OH_b) bond.

The CH-stretching transitions corresponding to $\Delta v_{CH} = 1-3$ are observed in the jet-cooled NID spectra of both catechol-d_0 and -d_2 as shown in Figures 2 and 6, respectively. Expanded figures of the CH-stretching regions in both the catechol-d_0 and -d_2 NID spectra are given as Supporting Information in Figures 4S−9S. Coupling between the aryl CH-stretching modes causes deviations from the simple isolated AO local mode model. The calculated fundamental harmonic CH-stretching frequencies given in Table 4 differ from the AO calculated frequencies in Table 6 due to the neglected coupling in the AO local mode model and the exclusion of anharmonicity in the harmonic frequencies. The fundamental CH-stretching region in the catechol-d_0 and -d_2 NID spectra is also somewhat different due to interaction with other molecular vibrations. We have shown that the effect of this coupling is negligible in the overtone regions and that the AO local mode model is suitable.[17,25] The $\Delta v_{CH} = 2$ region shows a broad band in the 5950−6060 cm^{-1}

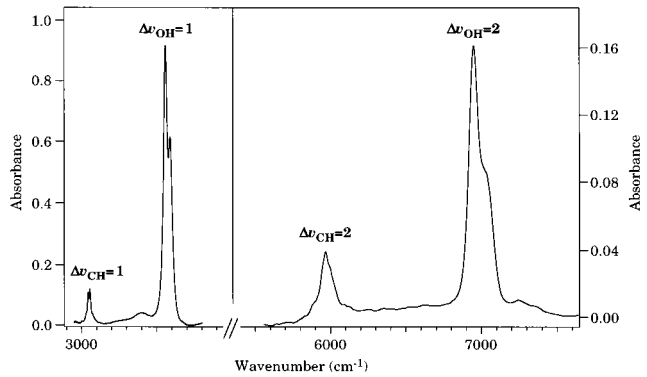

Figure 8. IR and NIR absorption spectra of catechol-d_0 dissolved in CS_2. The spectra were measured with a path length of 1 cm for the IR spectrum and 10 cm for the NIR spectrum.

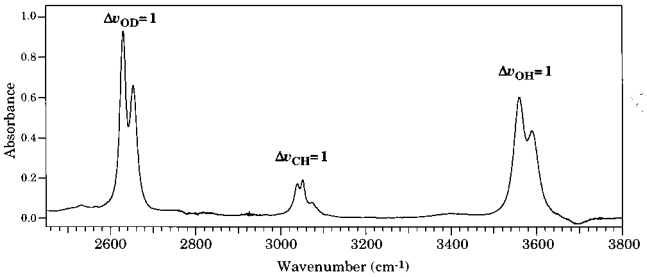

Figure 9. FT-IR spectrum of the catechol-d_1 and -d_2 mixture. The spectrum was measured at room temperature with a path length of 1 cm.

region with the strongest band at 6000 cm^{-1} in good agreement with the AO calculated positions of the CH_a-, CH_b-, and CH_c-stretching transitions (Table 6). In the $\Delta v_{CH} = 3$ region the S/N is about 2, however a broad Lorentzian-like band is visible centered around 8850 cm^{-1} in reasonable agreement with the AO calculation. A lower energy structure is possibly present at around 8670 cm^{-1} and could be an indication of the CH_d transition. It was not possible to observe any transitions in the $\Delta v_{CH} = 4$ region with NID spectroscopy.

Solution Phase Spectra. The spectrum of catechol-d_0 dissolved in CS_2 is shown in Figure 8 for the fundamental and the first overtone CH- and OH-stretching regions. The OH_b- and OH_f-stretching transitions are observed in both the $\Delta v_{OH} = 1$ and 2 regions. In the $\Delta v_{OH} = 3$ region, the OH_f peak position is not clearly resolved and its assignment is more uncertain. The observed OH-stretching frequencies in the catechol-d_0 CS_2 solution phase spectrum and the derived local mode parameters are given in Table 2. The spectrum of partially deuterated (~60% atom D) catechol dissolved in CS_2 was recorded in the 2500−9000 cm^{-1} region. In Figure 9 we show the fundamental OD-, CH-, and OH-stretching spectrum, which is similar to the NID spectrum of jet-cooled catechol-d_1 shown in Figure 7. The OD-stretching overtone regions have broad overlapping peaks, which have an increased uncertainty in the deconvolution. The observed OD-stretching frequencies and the derived local mode parameters are given in Table 3. The relatively large uncertainty in the OD local mode parameters are due to a lack of resolution in the $\Delta v_{OD} = 3$ region. Similar to the observation in the jet-cooled NID spectra, the OH-stretching transitions in the catechol-d_1 spectrum occur at the same frequency as the OH-stretching transitions in the catechol-d_0 spectrum, indicating that the coupling between the two hydroxyl groups is small.

Intensities. We have calculated the oscillator strengths of the CH- and OH-stretching transitions in catechol. The calculations have used the AO local mode model with the experimental or scaled ab initio local mode parameters and the HF/6-311++G(2d,2p) and the B3LYP/6-311++G(2d,2p) calculated DMFs. The calculated intensities obtained with the B3LYP/6-311++G(2d,2p) DMFs are given in Table 7. The intensities of the CH_a- and CH_d-stretching overtones are smaller than the intensities of the CH_b- and CH_c-stretching overtones. The intensity of the CH_d-stretching transition, which we expect to lie at lower frequency than the other three CH-stretch transitions, is significantly weaker than the sum of the other three in qualitative agreement with the observed spectrum of the $\Delta v_{CH} = 2$ and 3 regions. Within the Born−Oppenheimer approximation the DMF is not affected by deuteration. Thus we have used the calculated DMF to determine oscillator strengths of OD-stretching transitions in catechol-d_2. In Table 8 we compare the OH- and OD-stretching peak positions and intensities. Not surprisingly, the agreement with the experimental peak positions is good. The OD-stretching intensities are, as expected, weaker than the OH-stretching intensities, and the OD-stretching intensities decrease faster with increasing vibrational excitation than do the OH-stretching intensities due to the lower anharmonicity of the OD-stretching oscillators.

The observed and calculated relative intensities of the OH_b- to OH_f-stretching transitions are presented in Table 9. The experimentally determined intensity ratios agree to within approximately 20% for each of the overtones, less than the estimated experimental uncertainty. The NID spectra are not

TABLE 7: Calculated CH- and OH-Stretching Absolute Oscillator Strengths in Catechol[a]

v	CH_a	CH_b	CH_c	CH_d	OH_f	OH_b	exp
1	0.079	0.23	0.22	0.30	1.1	1.5	−5
2	0.78	0.85	0.84	0.53	7.0	5.8	−7
3	0.73	0.94	0.93	0.67	3.4	3.0	−8
4	0.50	0.71	0.67	0.48	1.7	1.9	−9

[a] Calculated with the B3LYP/6-311++G(2d,2p) DMFs and the experimental local mode parameters from Table 2 for the OH bonds and the local mode parameters from Table 5 for the CH bonds.

TABLE 8: Calculated OH and OD Peak Positions (in cm^{-1}) and Oscillator Strengths in Catechol-d_1 and -d_2[a]

	OH_f		OH_b		OD_f		OD_b		
v	$\tilde{\nu}$	f	$\tilde{\nu}$	f	$\tilde{\nu}$	f	$\tilde{\nu}$	f	exp[b]
1	3672	1.1	3614	1.5	2709	0.58	2667	0.81	−5
2	7177	7.0	7053	6.0	5329	2.7	5242	2.3	−7
3	10515	3.2	10319	3.2	7861	0.90	7725	0.87	−8
4	13686	1.7	13410	2.1	10304	0.32	10116	0.41	−9

[a] Calculated with experimental local mode parameters and the B3LYP/6-311++G(2d,2p) DMF. [b] Exponential factor for oscillator strengths.

TABLE 9: Intensity Ratios of OH_b- to OH_f-Stretching Transitions in Catechol[a]

	observed		calculated		
v	NID	CS_2/PAS	HF[d]	B3LYP[e]	B3LYP[f]
1	1.78	1.54[b]	1.27	1.41	1.40
2	1.86	1.99[b]	0.86	0.85	0.83
3	1.08	1.27[c]	1.02	0.95	0.89
4	0.59		1.28	1.21	1.11

[a] Intensity of OH_f-stretching transition set to 1. [b] From CS_2 solution phase spectrum. [c] From vapor phase ICL-PAS spectrum. [d] Calculated with NID experimental local mode parameters from Table 2 and the HF/6-311++G(2d,2p) DMF. [e] Calculated with NID experimental local mode parameters from Table 2 and the B3LYP/6-311++G(2d,2p) DMF. [f] Calculated with the calculated local mode parameters from Table 5 and the B3LYP/6-311++G(2d,2p) DMF.

TABLE 10: Intensity Ratios of OD_b- to OD_f-Stretching Transitions in Catechol-d_2[a]

	observed		calculated[b]	
υ	NID	CS_2	HF	B3LYP
1	1.17	1.32	1.26	1.39
2	0.96	1.15	0.86	0.85
3	0.85		1.03	0.96
4			1.30	1.26

[a] Intensity of OD_f-stretching transition set to 1. [b] Calculated with the NID experimental local mode parameters from Table 3 and the HF/6-311++G(2d,2p) and the B3LYP/6-311++G(2d,2p) DMFs.

corrected for laser power, so only comparison over small frequency ranges is reasonable. For $\Delta\upsilon_{OH} = 1$ and 2 the OH_b transitions are about a factor of 2 stronger than the OH_f transitions, for $\Delta\upsilon_{OH} = 3$ they are almost equal and for $\Delta\upsilon_{OH} = 4$ the OH_f transition is about a factor of 2 stronger. This is in contrast to other hydrogen-bonded systems. The fundamental hydrogen-bonded OH-stretching transition typically has significantly increased intensity[15] as seen, for example, in the water dimer.[26,39] The OH_b-stretching fundamental intensity in catechol is not significantly greater than the OH_f-stretching fundamental intensity and the OH_b-stretching intensity of the first overtone is strong; these two observations suggest that the intramolecular hydrogen bond in catechol is weak. In hydrogen-bonded clusters, our calculations predict the intensity of the first overtone of the hydrogen-bonded OH_b bond to be very weak due to a cancellation of the different contributions in the expansion of the DMF in eq 3.[26,28] The catechol hydrogen bond is very likely weaker than the theoretically predicted 4 kcal/mol, which is similar to the hydrogen-bond energy of the water dimer. The observed frequency shifts of the catechol OH_b bond also support the argument for a weak hydrogen bond.

We have previously found that overtone intensities are relatively insensitive to electron correlation, which also seems to be the case for catechol.[40] Calculation of intensities with experimentally or ab initio determined local mode parameters differ only slightly as seen in Table 9. The calculated OH_f to OH_b intensity ratios agree well with the observed ratios for $\Delta\upsilon_{OH} = 1$ and 3. However at $\Delta\upsilon_{OH} = 2$ the calculation underestimates the ratio by a factor of 2, whereas at $\Delta\upsilon_{OH} = 4$ the calculation overestimates the ratio by a factor of 2. Perhaps this illustrates the difficulty in calculating overtone intensities of hydrogen-bonded systems where the increase in fundamental intensity due to the increased first dipole moment derivative leads to a larger than usual cancellation of terms for the first and higher overtones. The observed and calculated OD_f to OD_b relative intensities are given in Table 10. There seems to be good agreement for both the fundamental transition, where the OD_b transition is slightly larger, and the overtone transitions, $\Delta\upsilon_{OD} = 2$ and 3, where the relative intensities are close to unity.

The observed and calculated relative CH− to OH-stretching intensities are listed in Table 11. The calculated relative overtone intensities are in good agreement with the observed intensity ratios from the CS_2 solution phase spectrum of catechol-d_0. For the fundamental region there is about a factor of 3 discrepancy. The HF and B3LYP methods give similar results.

We have determined total CH− or OH-stretching absolute oscillator strengths from the CS_2 solution phase spectra. The required equation for determining oscillator strengths in solution is given elsewhere.[41] Correction for the refractive index of the solution is necessary and we have used the refractive index of CS_2 ($n = 1.6319$)[42] and approximated it to be independent of

TABLE 11: Calculated and Observed Relative OH- to CH-Stretching Intensities in Catechol[a]

	expt[b]		calcd	
υ	CH	OH	CH	OH
1	1.0	13.1	1.0	3.1
2	1.0	4.2	1.0	4.3
3	1.0	2.1	1.0	1.9
4			1.0	1.5

[a] Calculated with the B3LYP/6-311++G(2d,2p) DMFs and local mode parameters from Table 2 for the OH bonds and Table 5 for the CH bonds. [b] From CS_2 solution phase spectra of catechol-d_0.

TABLE 12: Calculated Total CH- and OH−Stretching Oscillator Strengths

	ΣCH[a]		ΣOH[a]		
υ	obs.[b]	calc.[c]	obs.[b]	calc.[c]	exp
1	0.24	0.83	3.1	2.6	−5
2	1.8	3.0	7.5	13	−7
3	1.4	3.3	2.9	6.4	−8
4		2.4		3.6	−9

[a] Sum of intensities for all CH or OH bonds. [b] From CS_2 solution phase spectra of catechol-d_0. [c] Calculated with the B3LYP/6-311++G(2d,2p) DMFs and local mode parameters from Table 2 for the OH bonds and Table 5 for the CH bonds.

wavelength. The observed and calculated total CH- and OH-stretching absolute oscillator strengths agree well as seen in Table 12.

Line Widths. The OH-stretching transitions in jet-cooled catechol-d_0 shown in Figures 3−5 can be fitted well with a single Lorentzian band. As υ increases from $\Delta\upsilon_{OH} = 2$ to 4, the bandwidth of the OH_b transitions increases (4.3, 5.7, 6.0 cm^{-1}) whereas the bandwidth of the OH_f transitions remains relatively unchanged (3.3, 3.7, 3.5 cm^{-1}).

We have simulated the rotational band contour for the OH_b- and OH_f-stretching transitions as an asymmetric top. The OH_f-stretching vibration is almost parallel to the *b* principal axis, and we get a *b*-type rotational band, whereas the OH_b-stretching vibration lies between the *a* and *b* principal axes, and we obtain an *a*/*b*-type rotational band. The simulated rotational bands at 10 K and the molecular principal axes are shown in Figure 10. The band contour showed little change other than an overall increase in line width from about 2 cm^{-1} to about 4 cm^{-1} in the temperature range from 1 to 10 K. Each rotational transition was convoluted with a Gaussian with a fwhm of 0.1 cm^{-1}. The simulated rotational profiles are clearly not simple Lorentzians, so the observed bands cannot be simple rotational structure. We suggest that the observed band contour is due to intramolecular vibrational energy redistribution (IVR). The bandwidth difference between the OH_b- and OH_f-stretching transitions suggests that the IVR rate is not simply determined by the density of states. For example, the OH_b-stretching transition in the $\Delta\upsilon_{OH} = 3$ region lies 194 cm^{-1} lower than the OH_f-stretching transition, and thus the density of states in the bath would be very similar for the two transitions. However, the bandwidth of the OH_b-stretching transition is clearly larger than that of the OH_f-stretching transition. The same phenomenon is found in the other OH-stretching overtones and thus the bandwidth, i.e., the IVR rate, should be discussed in terms of specific "door way" states.

The difference in bandwidth between OH_b- and OH_f-stretching transitions may be interpreted by the model which explains the narrowing of width of CH overtones in benzene.[38] In benzene, the CH-stretching overtone line width increases with vibrational level until $\Delta\upsilon_{CH} = 5$, and then it decreases. The

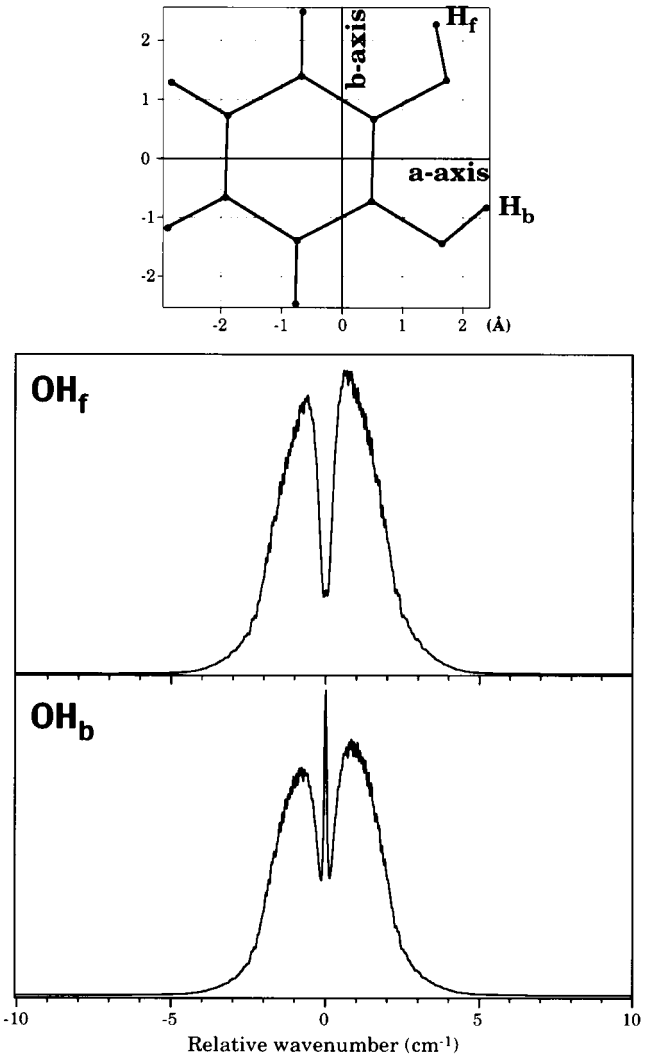

Figure 10. Simulation of the rotational contour of the OH_b- and OH_f-stretching transitions at 10 K. The principal molecular axes are also shown.

decrease in bandwidth is explained by the off-resonance between the CH-stretching overtone and the door way states. Due to anharmonicity, the spacing between successive vibrational energy levels decreases with increasing vibrational quanta and as a result the resonant condition is weakened by a larger energy gap. Thus, the narrower bandwidth of OH_f-stretching transitions in comparison to that of the OH_b-stretching transition suggests that OH_f-stretching energy levels are in a relatively off-resonant condition to the door way states, while the OH_b-stretching overtones always keep some resonant door way states.

The exact location and nature of these door way states and their coupling to the OH-stretching state determines the overall width and shape of the OH-stretching transitions. It is difficult to ascertain the exact door way states. The likely door way states are states that have one fewer quanta in the OH-stretching vibrations $|v - 1\rangle_{OH}$ combined with other vibrational modes. We attempted to investigate possible door way states of the form $|v - 1\rangle_{OH}|v_1\rangle|v_2\rangle$ (1:2) and $|v - 1\rangle_{OH}|v_1\rangle|v_2\rangle|v_3\rangle$ (1:3) where v_1, v_2, and v_3 are the quantum numbers of other vibrational modes in catechol. Comparison of the energy gap between successive overtones and the observed fundamental vibrational frequencies indicate that only very few $|v - 1\rangle_{OH}|v_1\rangle|v_2\rangle$ states are likely to act as door way states. The state $|3\rangle_{OH_b}|1\rangle_{8a}|1\rangle_{19a}$ has a predicted frequency of 13 404 cm^{-1} and is likely to strongly interact with the $|4\rangle_{OH_b}|0\rangle_{8a}|0\rangle_{19a}$ state at 13 406 cm^{-1}. Experimental frequencies for modes 8a and 19a were used.[5,13] The other possible interacting (1:2) states involved CH-stretching vibrations and lower frequency modes. However, all the normal modes with frequencies less than 722 cm^{-1} have been determined from solid-phase spectra or from ab initio calculations[13] and have significant uncertainty associated with them compared to our resolution in the NID spectra. Many of the possible (1:3) states also involve combination with these lower frequency normal modes. Furthermore, the frequencies required are not simply the fundamental vibrations, as these change slightly with vibrational excitation. Thus, determination of the exact door way states is, as mentioned, very difficult. However, we expect the line width is determined by a few door way or first tier states, which would couple to the second tier states, etc., and not just the density of states.

The line width of the OH-stretching transitions in the room-temperature ICL-PAS spectrum is about 30 cm^{-1}. This is similar to line widths observed in room-temperature vapor phase phenol spectra,[16] and significantly larger than the line width in the NID jet-cooled spectra, as expected. The band shape of the ICL-PAS peaks are not simple Lorentzians. One notable feature is the low energy shoulder on the OH_b transition as seen in Figure 4. We have investigated the effect of out-of-plane hydroxyl group rotation on the OH bond lengths. Rotation of the OH_b hydroxyl group is restricted by the intramolecular hydrogen-bonding interaction, whereas rotation of the OH_f hydroxyl group can occur more readily. A partial B3LYP/6-311++G(2d,2p) geometry optimization was performed with the OH_f bond rotated out of the plane of the molecule. The OH_f dihedral angle was frozen whereas all other degrees of freedom were relaxed. We found that the OH_b bond length increases steadily as the OH_f bond is rotated, from 0.964 Å at the minimum energy geometry to 0.966 Å in the geometry with the OH_f bond rotated 70 degrees out of the plane. On further rotation the OH_b bond length begins to decrease. This is not surprising, as it is expected that maximum overlap between the OH_b bond and the orbital corresponding to an oxygen lone pair will occur when the OH_f bond is about 60−70 degrees out of the plane of the molecule. This is similar to the tilt of the hydrogen acceptor H_2O unit in the water dimer.[26] The molecular energy increases with the OH_f rotation and is about 1.5 kcal/mol higher than the lowest energy conformer at 70 degrees rotation. At room temperature, there will be a contribution from molecules with the OH_f hydroxyl group rotation up to ±30 degrees from equilibrium geometry. Within this range the OH_f bond length changes by about 0.1 mÅ, whereas the OH_b bond length is elongated by up to 1 mÅ. Thus, a broader OH_b peak with low energy additional structure would be predicted, in agreement with the experimental spectrum.

In the jet-cooled NID spectrum we observe a significant difference between the line width of the CH- and OH-stretching transitions. The OH-stretching transitions are all less than 6 cm^{-1} wide. As mentioned the CH-stretching region is a relatively broad band. In the $\Delta v_{CH} = 3$ region, it is close to a Lorentzian with a fwhm of about 80 cm^{-1}. The larger line width of the CH-stretching band is also likely the reason we could not detect the transitions in the $\Delta v_{CH} = 4$ region, despite the similar calculated intensity of the CH- and OH-stretching transitions. The larger line width of the CH-stretching regions can be understood in terms of an increased number of possible door way states with larger coupling. There are more CH-stretching vibrations that couple with each other and with a larger number

of CH-bending modes. The CH bonds are also part of the aromatic ring, thus there will be additional coupling to the ring modes.

Conclusion

We have measured the OD-, CH-, and OH-stretching fundamental and overtone spectra of catechol-d_0, -d_1, and -d_2. We have used FT-IR and conventional absorption spectroscopy to measure the spectra of catechol dissolved in CS_2 and NID spectroscopy to measure the spectra of jet-cooled catechol. ICL-PAS was used to measure the room-temperature vapor phase spectrum of catechol-d_0 in the $\Delta v_{OH} = 3$ region. The spectra obtained from different experimental methods agree well with each other.

The overtone spectra clearly show that the two OH bonds are nonequivalent, in agreement with the suggested C_s symmetry of catechol. One OH bond forms a weak intramolecular hydrogen bond to the other oxygen atom. The OH-stretching transition associated with the hydrogen-bonded OH bond is red-shifted and the other OH bond transition is slightly blue-shifted compared to the OH-stretching frequency in phenol. Spectra of catechol-d_1 and ab initio frequency calculations indicate a weak coupling between the two OH bonds. Intensities of the transitions are calculated with an anharmonic oscillator local mode model and ab initio calculated dipole moment functions. The calculated and observed results agree well. Both the size of the red shift and the intensity pattern of the hydrogen-bonded OH bond suggest that catechol has a weak intramolecular hydrogen bond.

B3LYP calculations have previously been shown to have difficulties with hydrogen bonds. The results obtained from the HF and the B3LYP methods are similar, indicating that B3LYP appears appropriate to use for weak hydrogen bonds. The line width in the NID spectra of jet-cooled catechol is explained in terms of IVR and suggests a door way state model. The band shape in the room-temperature ICL-PAS spectrum suggests interaction between OH-stretching and OH rotation.

Acknowledgment. H.G.K. would like to thank IMS for kind hospitality during a visit. We are grateful to the Marsden fund administered by the Royal Society of New Zealand, University of Otago, a Grant-in-Aid for Scientific Research from the Ministry of Education, Culture, Sports, Science and Technology (MEXT), and the Daiko Foundation for financial support. The authors would like to thank Professor Alan Knight, Dr. Makoto Sakai, Dr. Morihisa Saeki, and Dr. Takeshi Watanabe for helpful discussions.

Supporting Information Available: *Supporting Information Available*: Two tables containing optimized geometries and calculated frequencies of catechol. Nine figures containing detailed spectra of OD- and CH-stretching transitions of catechol-d_0 and -d_2. This material is available free of charge via the Internet at http://pubs.acs.org.

References and Notes

(1) Caminati, W.; Di Bernardo, S.; Schäfer, L.; Kulp-Newton, S. Q.; Siam, K. *J. Mol. Struct.* **1990**, *240*, 263.
(2) Onda, M.; Hasunuma, K.; Hashimoto, T.; Yamaguchi, I. *J. Mol. Struct.* **1987**, *159*, 243.
(3) Brown, C. J. *Acta Crystallogr.* **1966**, *21*, 170.
(4) Wunderlich, V. H.; Mootz, D. *Acta Crystallogr. B* **1971**, *27*, 1684.
(5) Wilson, H. W. *Spectrochim. Acta* **1974**, *30A*, 2141.
(6) Greaves, S. J.; Griffith, W. P. *Spectrochim. Acta* **1991**, *47A*, 133.
(7) Ramírez, F. J.; López Navarette, J. T. *Vib. Spectrosc.* **1993**, *4*, 321.
(8) Tylli, H.; Konschin, H. *J. Mol. Struct.* **1979**, *57*, 13.
(9) Konschin, H.; Tylli, H. *J. Mol. Struct.* **1982**, *95*, 151.
(10) Fateley, W. G.; Carlson, G. L.; Bentley, F. F. *J. Phys. Chem.* **1975**, *79*, 199.
(11) Chung, G.; Kwon, O.; Kwon, Y. *J. Phys. Chem. A* **1997**, *101*, 9415.
(12) Vedernikova, I.; Proynov, E.; Salahub, D.; Haemers, A. *Int. J. Quantum Chem.* **2000**, *77*, 161.
(13) Gerhards, M.; Perl, W.; Schumm, S.; Henrichs, U.; Jacoby, C.; Kleinermanns, K. *J. Chem. Phys.* **1996**, *104*, 9362.
(14) Dietrich, S. W.; Jorgensen, E. C.; Kollman, P. A.; Rothenberg, S. *J. Am. Chem. Soc.* **1976**, *98*, 8310.
(15) *Theoretical Treatments of Hydrogen Bonding*; Hadzi, D., Ed.; John Wiley & Sons: Ltd.: Chichester, 1997.
(16) Davidsson, J.; Gutow, J. H.; Zare, R. N. *J. Phys. Chem.* **1990**, *94*, 4069.
(17) Kjaergaard, H. G.; Henry, B. R. *J. Phys. Chem.* **1995**, *99*, 899.
(18) Omi, T.; Shitomi, H.; Sekiya, N.; Takazawa, K.; Fujii, M. *Chem. Phys. Lett.* **1996**, *252*, 287.
(19) Ishiuchi, S.; Shitomi, H.; Takazawa, K.; Fujii, M. *Chem. Phys. Lett.* **1998**, *283*, 243.
(20) Hayward, R. J.; Henry, B. R. *J. Mol. Spectrosc.* **1975**, *57*, 221.
(21) Henry, B. R. *Acc. Chem. Res.* **1987**, *20*, 429.
(22) Child, M. S.; Halonen, L. *Adv. Chem. Phys.* **1984**, *57*, 1.
(23) Mortensen, O. S.; Henry, B. R.; Mohammadi, M. A. *J. Chem. Phys.* **1981**, *75*, 4800.
(24) Kjaergaard, H. G.; Yu, H.; Schattka, B. J.; Henry, B. R.; Tarr, A. W. *J. Chem. Phys.* **1990**, *93*, 6239.
(25) Kjaergaard, H. G.; Turnbull, D. M.; Henry, B. R. *J. Chem. Phys.* **1993**, *99*, 9438.
(26) Low, G. R.; Kjaergaard, H. G. *J. Chem. Phys.* **1999**, *110*, 9104.
(27) Kjaergaard, H. G.; Robinson, T. W.; Brooking, K. A. *J. Phys. Chem. A* **2000**, *104*, 11 297.
(28) Kjaergaard, H. G.; Low, G. R.; Robinson, T. W., unpublished.
(29) Henry, B. R.; Sowa, M. G. *Prog. Anal. Spectrosc.* **1989**, *12*, 349.
(30) Henry, B. R.; Kjaergaard, H. G.; Niefer, B.; Schattka, B. J.; Turnbull, D. M. *Can. J. Appl. Spectrosc.* **1993**, *38*, 42.
(31) Thomas, L. J., III.; Kelly, M. J.; Amer, N. M. *Appl. Phys. Lett.* **1978**, *32*, 736.
(32) Schattka, B. J.; Turnbull, D. M.; Kjaergaard, H. G.; Henry, B. R. *J. Phys. Chem.* **1995**, *99*, 6327.
(33) Atkins, P. W.; Friedman, R. S. *Molecular Quantum Mechanics*, 3rd ed.; Oxford University Press: Oxford, 1997.
(34) Kjaergaard, H. G.; Goddard, J. D.; Henry, B. R. *J. Chem. Phys.* **1991**, *95*, 5556.
(35) Frisch, M. J.; Trucks, G. W.; Schlegel, H. B.; Gill, P. M. W.; Johnson, B. G.; Robb, M. A.; Cheeseman, J. R.; Keith, T.; Petersson, G. A.; Montgomery, J. A.; Raghavachari, K.; Al-Laham, M. A.; Zakrzewski, V. G.; Ortiz, J. V.; Foresman, J. B.; Cioslowski, J.; Stefanov, B. B.; Nanayakkara, A.; Challacombe, M.; Peng, C. Y.; Ayala, P. Y.; Chen, W.; Wong, M. W.; Andres, J. L.; Replogle, E. S.; Gomperts, R.; Martin, R. L.; Fox, D. J.; Binkley, J. S.; Defrees, D. J.; Baker, J.; Stewart, J. P.; Head-Gordon, M.; Gonzalez, C.; Pople, J. A. Gaussian 94, Revision D.4; Gaussian Inc.: Pittsburgh, PA, 1995.
(36) Sowa, M. G.; Henry, B. R.; Mizugai, Y. *J. Phys. Chem.* **1991**, *95*, 7659.
(37) Foresman, J. B.; Frisch, A. *Exploring Chemistry with Electronic Structure Methods*, 2nd ed.; Gaussian, Inc.: Pittsburgh, PA, 1996.
(38) Reddy, K. V.; Heller, D. F.; Berry, M. J. *J. Chem. Phys.* **1982**, *76*, 2814.
(39) Huisken, F.; Kaloudis, M.; Kulcke, A. *J. Chem. Phys.* **1996**, *104*, 17.
(40) Kjaergaard, H. G.; Daub, C. D.; Henry, B. R. *Mol. Phys.* **1997**, *90*, 201.
(41) Howard, D. L.; Henry, B. R. *J. Phys. Chem. A* **1998**, *102*, 561.
(42) *CRC Handbook of Chemistry and Physics*; 64th ed.; Weast, R. C., Ed.; CRC Press: Boca Raton, FL, 1984.